



Constraints on ship  
NO<sub>x</sub> emissions in  
Europe using  
GEOS-Chem and OMI

G. C. M. Vinken et al.

# Constraints on ship NO<sub>x</sub> emissions in Europe using GEOS-Chem and OMI satellite NO<sub>2</sub> observations

G. C. M. Vinken<sup>1</sup>, K. F. Boersma<sup>1,2</sup>, A. van Donkelaar<sup>3</sup>, and L. Zhang<sup>4</sup>

<sup>1</sup>Department of Applied Physics, Eindhoven University of Technology, Eindhoven, the Netherlands

<sup>2</sup>Climate Observations, Royal Netherlands Meteorological Institute, De Bilt, the Netherlands

<sup>3</sup>Department of Physics and Atmospheric Science, Dalhousie University, Halifax, Canada

<sup>4</sup>Department of Atmospheric and Oceanic Sciences & Laboratory for Climate and Ocean-Atmosphere Studies, School of Physics, Peking University, Beijing 100871, China

Received: 7 June 2013 – Accepted: 26 June 2013 – Published: 23 July 2013

Correspondence to: G. C. M. Vinken (g.c.m.vinken@tue.nl)

Published by Copernicus Publications on behalf of the European Geosciences Union.

Title Page

Abstract

Introduction

Conclusions

References

Tables

Figures



Back

Close

Full Screen / Esc

Printer-friendly Version

Interactive Discussion



## Abstract

We present a top-down ship NO<sub>x</sub> emission inventory for the Baltic Sea, North Sea, Bay of Biscay and Mediterranean Sea, based on satellite observed tropospheric NO<sub>2</sub> columns of the Ozone Monitoring Instrument (OMI) for 2005–2006. We improved the representation of ship emissions in the GEOS-Chem chemistry transport model, and compared simulated NO<sub>2</sub> columns to consistent satellite observations. Relative differences between simulated and observed NO<sub>2</sub> columns have been used to constrain ship emissions in four European seas (Baltic Sea, North Sea, Bay of Biscay and Mediterranean Sea). The constrained ship tracks account for 39 % of total top-down European ship NO<sub>x</sub> emissions, which amounts to 0.96 TgN for 2005, and 1.0 TgN for 2006 (11–15 % lower than the bottom-up EMEP ship emission inventory). Our results indicate that EMEP emissions in the Mediterranean Sea are too high (by 60 %) and misplaced by up to 150 km, which can have important consequences for local air quality simulations. In the North Sea, our top-down emissions amount to 0.05 TgN for 2005 (35 % lower than EMEP). Increased top-down emissions were found for the Baltic Sea and Bay of Biscay, with emission totals of 0.05 TgN (131 % higher than EMEP) and 0.08 TgN for 2005 (128 % higher than EMEP), respectively. Our study explicitly accounts for the (non-linear) sensitivity of satellite retrievals to changes in the a priori NO<sub>2</sub> profiles. Although the effect of this sensitivity might be minor for small emission increments, our findings stress the need for consistent information in satellite retrieval and model, as satellite observations are never fully independent of model information (i.e. assumptions on vertical NO<sub>2</sub> profiles). Our study provides for the first time a space-based top-down ship NO<sub>x</sub> emission inventory, and can serve as a framework for future studies to constrain ship emissions using satellite NO<sub>2</sub> observations in other seas.

### Constraints on ship NO<sub>x</sub> emissions in Europe using GEOS-Chem and OMI

G. C. M. Vinken et al.

Title Page

Abstract

Introduction

Conclusions

References

Tables

Figures

⏪

⏩

◀

▶

Back

Close

Full Screen / Esc

Printer-friendly Version

Interactive Discussion



## 1 Introduction

Strong emissions of gases and particulate matter by ships affect the composition of the marine boundary layer, with important consequences for climate change, air quality and public health. Because hardly any regulations for the maritime sector exist in international waters, ships are still allowed to burn marine heavy fuel, resulting in substantial emissions of black carbon (BC), sulphur dioxide (SO<sub>2</sub>), nitrogen oxides (NO<sub>x</sub> = NO + NO<sub>2</sub>), and volatile organic compounds (VOCs) (e.g. Eyring et al., 2010). NO<sub>x</sub> and SO<sub>2</sub> emissions from ships are relatively high compared to emissions from other transport sectors because marine heavy fuel is high in sulphur content and is combusted at high temperatures without reduction technologies (Eyring et al., 2005). Recently, new legislation has been proposed that sets limits on sulphur and nitrogen oxide emissions from new ships in so-called sulphur emission control areas (SECAs) and NO<sub>x</sub> emissions control areas (NECAs). In Europe, SECAs are in effect since 2006 and 2007 for the North Sea and Baltic Sea, respectively, and a NECA is planned for the Baltic Sea for 2016. The North American coastal waters are designated as both a SECA and NECA since 2012 (IMO, 2009). Stringent emission limits for ships in these seas will be enforced in several steps, but the International Maritime Organization (IMO) is currently considering delaying the implementation of tighter limits in NECAs.

NO<sub>x</sub> emissions lead to O<sub>3</sub> and particulate matter formation, detrimental to air quality in the densely populated coastal regions close to ship lanes. Furthermore, O<sub>3</sub> influences the hydroxyl-radical (OH) concentrations that determine the lifetime of methane (CH<sub>4</sub>) (Lawrence and Crutzen, 1999), thereby influencing its global radiative forcing (IPCC, 2007). Sulphate (SO<sub>4</sub><sup>2-</sup>) formed by oxidation of sulfur dioxide (SO<sub>2</sub>) is the dominant aerosol from ship emissions and has a negative radiative forcing (due to its efficient reflection of sunlight). Aerosols originating from ships can also have an indirect (negative) effect on radiative forcing by altering the properties of clouds (e.g. Schreier et al., 2007; Lauer et al., 2007). Because of their important effect on both air quality

### Constraints on ship NO<sub>x</sub> emissions in Europe using GEOS-Chem and OMI

G. C. M. Vinken et al.

Title Page

Abstract

Introduction

Conclusions

References

Tables

Figures



Back

Close

Full Screen / Esc

Printer-friendly Version

Interactive Discussion



**Constraints on ship  
NO<sub>x</sub> emissions in  
Europe using  
GEOS-Chem and OMI**

G. C. M. Vinken et al.

Title Page

Abstract

Introduction

Conclusions

References

Tables

Figures

⏪

⏩

◀

▶

Back

Close

Full Screen / Esc

Printer-friendly Version

Interactive Discussion

and climate, ship emissions have received increasing attention over the past years. Previous studies (e.g. Corbett et al., 2007; Eyring et al., 2010; Paxian et al., 2010) proposed that global ship NO<sub>x</sub> emissions amount to 3.0–10.4 TgN per year (15–35 % of global anthropogenic NO<sub>x</sub> emissions). However, as individual measurements of ship emissions are sparse, and knowledge of activity, technology and global fleet is limited, these bottom-up inventories suffer from large uncertainties, making it difficult to assess the efficacy of reducing ship emissions in order to mitigate the effects of air pollution and climate change.

The magnitude and geographic location of ship NO<sub>x</sub> emissions can be constrained by using high spatial resolution satellite observations of NO<sub>2</sub> columns. Previous studies have demonstrated this concept, where satellite observed NO<sub>2</sub> columns, in combination with simulations from a chemistry transport model (CTM), were used to constrain NO<sub>x</sub> emissions. For example, Martin et al. (2003) used observations from the Global Ozone Monitoring Experiment (GOME) instrument to scale global NO<sub>x</sub> emissions in the GEOS-Chem CTM. Different instruments have since then been used to constrain various source categories: anthropogenic emissions (e.g. Martin et al., 2006), soil NO<sub>x</sub> (e.g. Jaeglé et al., 2005) and lightning NO<sub>x</sub> (e.g. Boersma et al., 2005). Recently Wang et al. (2012) used high resolution NO<sub>2</sub> columns from the Ozone Monitoring Instrument (OMI) to detect newly built power plants in China.

Satellite observations have also provided information on ship pollution. Beirle et al. (2004) used GOME measurements of tropospheric NO<sub>2</sub> columns to estimate emissions in the ship lane from Sri Lanka to Indonesia. Several ship tracks were identified in global maps of satellite observed NO<sub>2</sub> columns from the SCanning Imaging Absorption spectroMeter for Atmospheric CartographY (SCIAMACHY) and compared to an emission inventory by Richter et al. (2004). Marmer et al. (2009) took advantage of the higher spatial and temporal resolution of OMI NO<sub>2</sub> observations of the ship track in the Mediterranean Sea to assess several emissions inventories. A trend in NO<sub>2</sub> columns over 4 ship tracks in Europe and Asia, following the rhythm of global economic activity, was shown by de Ruyter de Wildt et al. (2012) using GOME, SCIAMACHY, OMI

**Constraints on ship  
NO<sub>x</sub> emissions in  
Europe using  
GEOS-Chem and OMI**

G. C. M. Vinken et al.

Title Page

Abstract

Introduction

Conclusions

References

Tables

Figures

⏪

⏩

◀

▶

Back

Close

Full Screen / Esc

Printer-friendly Version

Interactive Discussion

and GOME-2 observations. Franke et al. (2009) used a combination of observed NO<sub>2</sub> columns of SCIAMACHY, GOME and GOME-2 instruments and modelled columns using the ECHAM5/MESSy1 CTM to evaluate ship NO<sub>x</sub> emissions in the ship track from Sri Lanka to Indonesia. They concluded that their modelled NO<sub>2</sub> columns were in good agreement with observed columns for 2002–2007. However, as most CTMs, their model neglected the in-plume chemistry of ship emissions by instantly diluting the emissions over the model grid cell. This results in an overestimation of modelled NO<sub>x</sub> concentrations (e.g. Kasibhatla et al., 2000; Davis et al., 2001; Vinken et al., 2011), and therefore in too low ship NO<sub>x</sub> emissions estimates. Various methods have been proposed in literature to account for the non-linear chemistry during the first stages of ship plume expansion (for a review see Paoli et al., 2011). Here we use our recently developed method using a plume-in-grid approach (Vinken et al., 2011) that accounts for the non-linear in-plume chemistry in the GEOS-Chem global 3-D CTM. Compared to instant dilution of ship emissions, this method leads to lower (simulated) background NO<sub>x</sub> concentrations over the North Atlantic ocean by up to 60%.

In this study we focus on providing top-down constraints on ship NO<sub>x</sub> emissions by comparing modelled and satellite-observed NO<sub>2</sub> columns for four major ship routes in Europe (Mediterranean Sea, Bay of Biscay, Baltic Sea and North Sea). This is the first time that NO<sub>2</sub> pollution is evaluated using satellite measurements over the Bay of Biscay, Baltic Sea and North Sea. These observed columns are compared to NO<sub>2</sub> columns simulated with the nested version of the GEOS-Chem CTM. The high resolution (1/2° × 2/3°) of the nested version of GEOS-Chem is capable of resolving major ship tracks in Europe, and improves the localization of emissions. We run the European nested version of GEOS-Chem at a 1/2° × 2/3° resolution for 2005–2006 using the plume-in-grid treatment of ship NO<sub>x</sub> emissions introduced in Vinken et al. (2011). Using the combination of the high-resolution modelled columns and OMI observed columns, we present for the first time space-based, seasonal and annual constraints on ship NO<sub>x</sub> emissions in four major European ship routes for 2005–2006.

## 2 Simulations and satellite observations of tropospheric NO<sub>2</sub> columns

### 2.1 GEOS-Chem model

Here we use the GEOS-Chem (v8-03-02; <http://geos-chem.org>) chemistry transport model to simulate tropospheric NO<sub>2</sub> columns over Europe for 2005–2006. The nested grid version of GEOS-Chem (Wang et al., 2004; Chen et al., 2009; Zhang et al., 2012) is operated at 1/2° × 2/3° resolution with 47 vertical layers, and a transport and chemistry time step of 10 and 20 min, respectively. The boundary conditions are updated every 3 h using global simulations from the 2° × 2.5° parent model (one-way nesting). Both the nested and global simulations are driven by GEOS-5 assimilated meteorological observations from the NASA Global Modeling and Assimilation Office (GMAO). The nested grid domain extends from 30 to 70° N and 30° W to 50° E. The lowermost layer of the model has a approximate depth of 120 m and a vertical extent of 80 km. GEOS-Chem has a detailed simulation of ozone-NO<sub>x</sub>-hydrocarbon-aerosol chemistry, as recently described and discussed by Mao et al. (2010) and Lin et al. (2012). The reactive uptake coefficient  $\gamma_{\text{N}_2\text{O}_5}$  for N<sub>2</sub>O<sub>5</sub> in aerosols is from Macintyre and Evans (2010), with a resulting annual mean value for 2005 of  $\gamma_{\text{N}_2\text{O}_5}$  in surface air over our domain of 0.004, at the high end of recently measured values (0.0005–0.006; Brown et al., 2009; Bertram et al., 2009). We performed a spin-up of one year (2004) and simulations for 2005–2006. Daily simulated tropospheric NO<sub>2</sub> columns corresponding to the satellite overpass time (between 13:00 and 15.00 LT) were averaged. To ensure consistency with the satellite observations, only days with valid satellite observations (see next section) were included.

Global anthropogenic emissions are from EDGAR (Olivier and Berdowski, 2001). Over Europe these are replaced with the Monitoring and Evaluation of the Long-range Transmission of Air Pollutants in Europe (EMEP) inventory (Vestreng et al., 2007). We replaced ship emissions (NO<sub>x</sub>, SO<sub>2</sub> and CO) from the EMEP inventory by a combination of the EMEP and (global) AMVER-ICOADS (Wang et al., 2008) inventories, as emissions were misplaced in the EMEP inventory (see discussion in Sect. 3.1).

### Constraints on ship NO<sub>x</sub> emissions in Europe using GEOS-Chem and OMI

G. C. M. Vinken et al.

Title Page

Abstract

Introduction

Conclusions

References

Tables

Figures

⏪

⏩

◀

▶

Back

Close

Full Screen / Esc

Printer-friendly Version

Interactive Discussion



## Constraints on ship NO<sub>x</sub> emissions in Europe using GEOS-Chem and OMI

G. C. M. Vinken et al.

Title Page

Abstract

Introduction

Conclusions

References

Tables

Figures

⏪

⏩

◀

▶

Back

Close

Full Screen / Esc

Printer-friendly Version

Interactive Discussion

NO<sub>x</sub> emissions from soils are included based on the parametrization of Yienger and Levy II (1995) and Wang et al. (1998). Furthermore, lightning (Sauvage et al., 2007), biomass burning (van der Werf et al., 2006), biofuel (Yevich and Logan, 2003) and aircraft (Baughcum et al., 1996) NO<sub>x</sub> emissions are included in the model. An overview of the total NO<sub>x</sub> emissions over Europe for 2005–2006 used in this study is given in Table 1. Anthropogenic sources (7.2 Tg N yr<sup>-1</sup>; including aircraft, biofuel, fertilizer use and ships) account for 87 % of the total NO<sub>x</sub> emissions in 2005. Natural emissions (biomass burning, lightning and soil) peak in summer, accounting for 25 % of total European NO<sub>x</sub> emissions in July and August 2005.

We use the plume-in-grid approach developed by Vinken et al. (2011) to take into account non-linear chemistry occurring in ship plumes immediately after emission. In this approach a Gaussian plume model with chemistry has been used to construct a lookup table (LUT), that contains the fraction of NO<sub>x</sub> remaining and (net) O<sub>3</sub> produced in 5 h of plume expansion after emission as a function of several environmental parameters. In this study we extend this method in two ways. First, we limit the chemical aging time in the expanding plume model to 2.5 h, as the plume typically grows to the size of the model grid cell (1/2° × 2/3°) within this time. The resulting NO<sub>x</sub> concentrations in (GEOS-Chem) grid cells with ship emissions can be considered as background concentrations, i.e. representative for NO<sub>x</sub> concentrations after a ship passed by 2.5 h earlier. Because we will compare the simulated columns with satellite observed NO<sub>2</sub> columns, which also include contributions from emissions that occurred during the past 2.5 h, we need to take these into account as well. Therefore, we extended our plume-in-grid approach by application of the fraction of NO<sub>x</sub> remaining after 2 and 1 h plume expansion, and just prior to observation (after 15 min expansion). The fractions of NO<sub>x</sub> remaining are then multiplied with the emissions over the last 2.5 h (Fig. 1a). These emissions are added to the NO<sub>x</sub> concentration in the grid cell (Fig. 1b) and the resulting tropospheric columns are stored, to allow a fair comparison between the satellite observations (sensitive to all recent emissions) and GEOS-Chem. Note that the ship emissions from the last 2.5 h are not propagated in the regular model chemistry, as

these represent emissions subject to non-linear plume chemistry, but only serve as a model snapshot that is representative of what the satellite observes.

To evaluate our method, we compared tropospheric  $\text{NO}_2$  columns to the conventional approach where all  $\text{NO}_x$  is assumed to be instantly diluted over the grid cell.

Figure 1b shows that our simulation with the plume-in-grid approach and accounting for fresh emissions leads to a higher column than instant dilution. This is because just after initial release in the plume, OH concentrations are much suppressed, resulting in a longer  $\text{NO}_2$  lifetime (during the first part of expansion). However, this is not always the case. Figure 2 shows that, depending on ambient conditions (e.g. background  $\text{NO}_x$  and  $\text{O}_3$  concentrations), the fraction of  $\text{NO}_x$  remaining can be either higher (Fig. 2a) or lower (Fig. 2b) than predicted by instant dilution. For the first hours of expansion, OH is suppressed in the plume, and the  $\text{NO}_2$  lifetime is longer for the expanding plume (solid line) compared to instant dilution of emissions (dashed line). If  $\text{NO}_x$ ,  $\text{O}_3$  concentrations are relatively high (0.6 and 60 ppbv, respectively; Fig. 2a), instant dilution of emissions results in a lower fraction of  $\text{NO}_x$  remaining compared to an expanding plume simulated by the PARANOX Gaussian plume model (Vinken et al., 2011). For relative clean ambient conditions,  $\text{NO}_x$ ,  $\text{O}_3$  concentrations of 0.15 and 39 ppbv, respectively (Fig. 2b), instant dilution results in a higher fraction of  $\text{NO}_x$  remaining, as in this case the higher  $\text{NO}_x$  concentrations in the plume lead to efficient OH formation and a lower  $\text{NO}_x$  lifetime. Figure 2b is consistent with a recent study by Valin et al. (2011), who showed, using a 2-D plume model,  $\text{NO}_2$  columns for a  $2 \times 2 \text{ km}^2$  (i.e. “plume” size) simulation could be higher (by up to 35 %), compared to  $48 \times 48 \text{ km}^2$  (instant dilution scale) resolution simulations, for an moderate emission strength. Furthermore, we note that horizontal transport of emissions in the 2.5 h of expansion is not included in Fig. 1b, while for instant dilution there is transport out of the grid cell in this time, resulting in a lower column. The effect of this transport on our final constraints is minor, as we use long temporal averages and use enhanced  $\text{NO}_2$  from ship emissions extended over multiple grid cells. Although the plume-in-grid approach presented in this work will probably introduce additional model errors, it takes into account non-linear chemistry

Constraints on ship  
 $\text{NO}_x$  emissions in  
Europe using  
GEOS-Chem and OMI

G. C. M. Vinken et al.

Title Page

Abstract

Introduction

Conclusions

References

Tables

Figures



Back

Close

Full Screen / Esc

Printer-friendly Version

Interactive Discussion





in expanding ship emission plumes, allowing for an appropriate comparison of satellite observations and model simulations of aged pollution plumes.

## 2.2 Ozone Monitoring Instrument

The Dutch–Finish Ozone Monitoring Instrument (OMI) is a nadir-viewing solar backscatter imaging spectrograph aboard the Aura satellite, measuring in the range 264 to 504 nm (Levelt et al., 2006). Aura was launched in sun-synchronous polar orbit on 15 July 2004 with a local equator-crossing time of 13:40 h. OMI measurements have a spatial resolution up to 13 km × 24 km for nadir pixels and provide daily global coverage. We use the tropospheric NO<sub>2</sub> vertical column densities from Dutch OMI tropospheric NO<sub>2</sub> (DOMINO) v2.0 product (available from the Tropospheric Emissions Monitoring Internet Service (TEMIS); <http://www.temis.nl>). The DOMINO v2.0 product includes improvements in the radiative transfer modelling, high-resolution surface albedo climatology, better a priori TM4 NO<sub>2</sub> vertical profiles and high-resolution terrain height (Hains et al., 2010; Boersma et al., 2011). The uncertainty in OMI observed columns due to spectral fitting is  $0.7 \times 10^{15}$  molecules cm<sup>-2</sup> and dominates the overall retrieval error over oceans and remote areas (Boersma et al., 2007). Errors arising from incorrect assumptions on surface albedo, aerosols, clouds or the NO<sub>2</sub> vertical profile dominate the overall retrieval error over polluted regions (Boersma et al., 2004). The total error budget for DOMINO v2.0 is estimated to be  $1.0 \times 10^{15}$  molecules cm<sup>-2</sup> + 25 % (Boersma et al., 2011). Recently, Irie et al. (2012) showed that only a small bias ( $-10 \pm 14$  %) exists between DOMINO v2.0 retrievals and in-situ Multi-Axis Differential Optical Absorption Spectroscopy (MAX-DOAS) observations at several sites in Japan and China.

OMI retrieves slant columns; the integrated abundance of NO<sub>2</sub> along the average photon path through the atmosphere to the instrument. These slant columns are converted to (tropospheric) vertical column densities (VCDs) using a (tropospheric) air mass factor (AMF). This AMF, and hence the retrieved tropospheric NO<sub>2</sub> VCD, is sensitive to the a priori vertical NO<sub>2</sub> profile. In the DOMINO v2.0 retrieval (from now on

### Constraints on ship NO<sub>x</sub> emissions in Europe using GEOS-Chem and OMI

G. C. M. Vinken et al.

Title Page

Abstract

Introduction

Conclusions

References

Tables

Figures

◀

▶

◀

▶

Back

Close

Full Screen / Esc

Printer-friendly Version

Interactive Discussion



## Constraints on ship NO<sub>x</sub> emissions in Europe using GEOS-Chem and OMI

G. C. M. Vinken et al.

Title Page

Abstract

Introduction

Conclusions

References

Tables

Figures

⏪

⏩

◀

▶

Back

Close

Full Screen / Esc

Printer-friendly Version

Interactive Discussion

called DOMINO2), NO<sub>2</sub> vertical profiles simulated by TM4 (Dentener et al., 2003) are used. These vertical profiles have a native spatial resolution of 2° × 3°, which is improved upon by spatial interpolation to the OMI pixel center. Here we replace these a priori vertical NO<sub>2</sub> profiles with profiles from GEOS-Chem nested grid simulations (1/2° × 2/3° horizontal resolution) for the same day and (overpass) time of the OMI measurement, and calculate new tropospheric AMFs. Application of these new tropospheric AMFs results in a new dataset of tropospheric VCDs (from now on called DOMINO2\_GC), allowing a consistent comparison of the OMI observed columns with GEOS-Chem simulated columns, because the vertical distribution assumed in the retrieval is now the same as predicted by the model. The effect of these high-resolution GEOS-Chem profiles will be discussed in the next section.

We exclude clouded situations and snow or ice covered pixels to limit retrieval errors, by filtering pixels with cloud radiance fraction above 0.5, and surface albedo above 0.2. The effective cloud fraction is from the OMI O<sub>2</sub>-O<sub>2</sub> retrieval (OMCLDO2) (Acarreta et al., 2004; Sneep et al., 2008), and OMI surface albedos are from Kleipool et al. (2008). We removed the outer 2 (large) pixels on each side of the swath to reduce spatial smearing due to viewing geometry. OMI pixels are regridded to the GEOS-Chem nested horizontal grid (1/2° × 2/3°), requiring a grid cell coverage of over 75% and more than 3 observations per monthly/seasonal average. A 1 yr averaged map of OMI tropospheric NO<sub>2</sub> columns is shown in Fig. 3 for 2005.

### 2.3 Evaluation of GEOS-Chem and OMI tropospheric NO<sub>2</sub> columns

We compare GEOS-Chem simulations of tropospheric NO<sub>2</sub> columns with OMI observed columns (both DOMINO2 and DOMINO2\_GC) for 2005 (Fig. 3 and 4). Spatial patterns between DOMINO2\_GC and GEOS-Chem for these annual averages over the entire domain are highly consistent ( $R^2 = 0.90$ ,  $n = 9270$ ), but the simulated columns are lower than DOMINO2\_GC over urban and industrial areas. Although the observations show stronger seasonal variation for 2005–2006 (Fig. 4), the temporal correlation between GEOS-Chem and DOMINO2\_GC monthly means ( $R^2 = 0.95$ ) is re-

**Constraints on ship  
NO<sub>x</sub> emissions in  
Europe using  
GEOS-Chem and OMI**

G. C. M. Vinken et al.

Title Page

Abstract

Introduction

Conclusions

References

Tables

Figures

⏪

⏩

◀

▶

Back

Close

Full Screen / Esc

Printer-friendly Version

Interactive Discussion

markably strong, with a root-mean-square-error (RMSE) of  $0.24 \times 10^{15}$  molec cm<sup>-2</sup>. For GEOS-Chem and DOMINO2 the temporal correlation is  $R^2 = 0.89$ , with a RMSE of  $0.45 \times 10^{15}$  molecules cm<sup>-2</sup>. Differences between DOMINO2\_GC and DOMINO2 arise from the different a priori NO<sub>2</sub> profiles used in the air mass factor (AMF) calculation.

5 GEOS-Chem NO<sub>2</sub> profiles differ in three ways from the original TM4 profiles: (1) different emissions over the domain, (2) higher spatial resolution and (3) different CTM (e.g. different vertical mixing and chemical lifetime). Different emissions most likely dominate the changes in AMFs. TM4 used emissions from the POET-project (Precursors of Ozone and their Effects on the Troposphere) for the year 1997 (Olivier et al., 2003), which amount to  $8.2 \text{ Tg N yr}^{-1}$  for Europe. In GEOS-Chem we use EMEP (Vestreng et al., 2007) emissions, which amount to  $6.3 \text{ Tg N yr}^{-1}$  for 2005. Lower emissions lead to lower concentrations in the a priori profiles, and hence higher AMFs, resulting in lower tropospheric NO<sub>2</sub> columns (e.g. Martin et al., 2003; Boersma et al., 2004).

15 OMI NO<sub>2</sub> retrievals using GEOS-Chem NO<sub>2</sub> profiles in the AMF calculation are on average 10 % lower than the original DOMINO2 retrievals using TM4 a priori NO<sub>2</sub> profiles. The new DOMINO2\_GC retrievals and GEOS-Chem now agree to within 7 %, with largest differences in winter months. The wintertime underestimation of GEOS-Chem shown in Fig. 4 possibly reflects a too short NO<sub>2</sub> chemical lifetime in GEOS-Chem as suggested by a number of recent studies into reaction rate updates (e.g. Stavrou et al., 2013; Zhang et al., 2012). In particular the value for the uptake coefficient  $\gamma_{\text{N}_2\text{O}_5}$  in GEOS-Chem is high compared to recent laboratory and field estimates of this value (e.g. Brown et al., 2009; Mollner et al., 2010; Henderson et al., 2012; Butkovskaya et al., 2007, 2009). We conclude that the nested GEOS-Chem CTM is in close agreement with OMI observed NO<sub>2</sub> columns over Europe. Differences in wintertime between

25 OMI and GEOS-Chem are unlikely to influence our results because of our filter criteria (discussed in the next section).

## 2.4 Selection of OMI NO<sub>2</sub> observations

Figure 3a (top) shows two ship tracks in the annual averaged OMI NO<sub>2</sub> observations; one in the Bay of Biscay and one in the Mediterranean Sea. Emission inventories (see next section) suggest that there are also busy ship routes in the North Sea. However, detection of ship tracks in this sea presents significant challenges, since influence from outflow of pollution from land source regions often prohibits a clear view of the source of interest. To be able to detect ship emissions in this sea, we inspect daily OMI observations and screen out all days with measurements that are significantly affected by continental outflow (e.g. Fig. 5a). Furthermore, we filter for days that have cloud-free observations over the entire ship track area (Fig. 5b), as scattered clouds prevent the unambiguous detection of pollution from ships. Using these two criteria we can now identify two additional ship tracks in European seas (Baltic Sea and North Sea) (Fig. 5c).

## 3 Top-down ship emission estimates

### 3.1 Ship emission inventories

In the GEOS-Chem CTM two (recent) ship emission inventories can be used for Europe; the European regional EMEP inventory (Vestreng et al., 2007) and the global AMVER-ICOADS inventory (Wang et al., 2008). The left panels of Fig. 6 show the spatial distribution of European ship NO<sub>x</sub> emissions, with totals for the EMEP and AMVER-ICOADS inventory for 2005 of 1.1 TgN and 0.8 TgN, respectively. Differences between these inventories arise from the use of different methodologies (e.g. using fuel consumption versus shipping activity) and spatial allocation. The AMVER-ICOADS inventory is based on international fuel statistics, which do not include fuel consumed for domestic traffic, whereas EMEP does include these domestic emissions. Therefore AMVER-ICOADS underestimates ship emissions over inland seas and coastal

## Constraints on ship NO<sub>x</sub> emissions in Europe using GEOS-Chem and OMI

G. C. M. Vinken et al.

[Title Page](#)[Abstract](#)[Introduction](#)[Conclusions](#)[References](#)[Tables](#)[Figures](#)[⏪](#)[⏩](#)[◀](#)[▶](#)[Back](#)[Close](#)[Full Screen / Esc](#)[Printer-friendly Version](#)[Interactive Discussion](#)

## Constraints on ship NO<sub>x</sub> emissions in Europe using GEOS-Chem and OMI

G. C. M. Vinken et al.

Title Page

Abstract

Introduction

Conclusions

References

Tables

Figures

◀

▶

◀

▶

Back

Close

Full Screen / Esc

Printer-friendly Version

Interactive Discussion



zones with significant domestic ship traffic, like the (eastern part of the) Mediterranean Sea (Marmer et al., 2009). The spatial allocation in EMEP is based on the distance each ship covers between ports, information provided by the Lloyd's Register of Shipping (Vestreng, 2003). In the AMVER-ICOADS inventory the spatial allocation is taken from actual ship locations reported to the Automated Mutual-Assistance Vessel Rescue System (AMVER) and International Comprehensive Ocean-Atmosphere Data Set (ICOADS). Comparison with annual OMI NO<sub>2</sub> observations (Fig. 6b) for the eastern part of Mediterranean Sea shows that the AMVER-ICOADS inventory (Fig. 6c) simulates the ship track closer to the observed tracks. The location of the EMEP emissions is misplaced by up to 150 km (too close to Crete, Fig. 6a). However, as the EMEP inventory does include domestic ship traffic, we combine both inventories and generate a new ship emission inventory (Fig. 6d). This inventory is based on EMEP emission totals, and AMVER-ICOADS emission locations for the eastern part of the Mediterranean Sea. In the following, we will use the combined EMEP & AMVER-ICOADS database as the a-priori emission inventory in our simulations.

### 3.2 Sensitivity of GEOS-Chem NO<sub>2</sub> columns to NO<sub>x</sub> emissions

Within pollution plumes, the NO<sub>x</sub> lifetime is influenced by the local NO<sub>x</sub> concentration. This is because oxidation losses depend on in-plume OH availability, which is determined by the local concentration of pollution, e.g. the NO<sub>x</sub> concentration itself. We need to account for this non-linear feedback when changing NO<sub>x</sub> emissions based on observed (changes in) NO<sub>2</sub> columns. Lamsal et al. (2011) introduced a dimensionless factor  $\beta$ , that represents the (modelled) sensitivity of NO<sub>2</sub> column changes to NO<sub>x</sub> emissions changes.  $\beta$  is computed by changing NO<sub>x</sub> emissions by a fixed prescribed percentage and evaluating the local (relative) change in NO<sub>2</sub> column:

$$\beta = \frac{\Delta E/E}{\Delta N_{\text{GC}}/N_{\text{GC}}} \quad (1)$$

## Constraints on ship NO<sub>x</sub> emissions in Europe using GEOS-Chem and OMI

G. C. M. Vinken et al.

Title Page

Abstract

Introduction

Conclusions

References

Tables

Figures

⏪

⏩

◀

▶

Back

Close

Full Screen / Esc

Printer-friendly Version

Interactive Discussion

with  $E$  the NO<sub>x</sub> emissions,  $N_{GC}$  the simulated tropospheric NO<sub>2</sub> column,  $\Delta E$  the change in NO<sub>x</sub> emissions, and  $\Delta N_{GC}$  the subsequent change in simulated tropospheric NO<sub>2</sub> column. Lamsal et al. (2011) found a global mean  $\beta$  value of 1.16 when perturbing emissions by 15%.  $\beta$  tends to be greater than one in remote areas with relatively low NO<sub>2</sub> concentrations, reflecting efficient OH production and a lower NO<sub>x</sub> lifetime following an increase in emissions. In polluted areas,  $\beta$  tends to be less than one as an increase in NO<sub>x</sub> will consume OH and increase the NO<sub>x</sub> lifetime. Recently, Lu and Streets (2012) showed a decrease of  $\beta$  values from about 2 to 0.7 over Indian power plants during 1996–2010, following a dramatic increase in NO<sub>x</sub> emissions. Their study illustrates the strong variability of  $\beta$ , and the need to determine  $\beta$  for a realistic emission strength. As we expect our ship emissions to change by more than 15% we follow a two-step approach to calculate  $\beta$  values, different from Lamsal et al. (2011). First we run our model with constrained emissions derived from the relative difference of observed and simulated NO<sub>2</sub> columns (ignoring the non-linear feedback of emission on simulated columns). From the results of these simulations we calculate  $\beta$  values for our ship tracks and apply these to derive new top-down emissions. We find  $\beta$  values of 0.3–0.9 (Table 2), indicating that emission changes lead to substantial changes in NO<sub>2</sub> columns over the ship lanes. This is expected, as ship emissions are released following our plume-in-grid approach, and NO<sub>x</sub> concentrations will be relatively high in the expanding plume, a situation comparable to release of NO<sub>x</sub> in a polluted area.

### 3.3 Sensitivity of OMI NO<sub>2</sub> columns to a priori (GEOS-Chem) NO<sub>2</sub> columns

OMI tropospheric NO<sub>2</sub> columns depend on the a priori vertical NO<sub>2</sub> profile. In this study we replaced the TM4 profiles used in the DOMINO v2.0 retrieval by high-resolution GEOS-Chem simulated NO<sub>2</sub> profiles (Sect. 2.2, leading to OMI NO<sub>2</sub> retrievals 10% lower than original DOMINO2). As a result of constraining ship emissions in GEOS-Chem, the retrieved OMI NO<sub>2</sub> columns will also change in response to updated a priori NO<sub>2</sub> profiles over the shipping lanes. We quantify the effect of changing GEOS-Chem NO<sub>2</sub> columns (NO<sub>x</sub> emissions) on OMI NO<sub>2</sub> columns by introducing a dimensionless

factor  $\gamma$ :

$$\gamma = \frac{\Delta N_{\text{OMI}}/N_{\text{OMI}}}{\Delta N_{\text{GC}}/N_{\text{GC}}} \quad (2)$$

with  $N_{\text{GC}}$  the simulated tropospheric  $\text{NO}_2$  column corresponding to the a priori profile shape used in the retrieval,  $N_{\text{OMI}}$  the retrieved OMI tropospheric  $\text{NO}_2$  column,  $\Delta N_{\text{GC}}$  the change in simulated  $\text{NO}_2$  column as a result of changing emissions, and  $\Delta N_{\text{OMI}}$  the change in retrieved  $\text{NO}_2$  column because of the changed a priori  $\text{NO}_2$  profile. A  $\gamma$  value of zero would indicate no sensitivity of OMI  $\text{NO}_2$  columns to changing GEOS-Chem columns. We calculate  $\gamma$  values in the same way as  $\beta$  values, using results of a model run with constrained emissions.  $\gamma$  is found to be always smaller than 1 (Table 2), indicating that OMI  $\text{NO}_2$  columns never change more than the GEOS-Chem columns. The  $\gamma$  factor illustrates that OMI retrievals are never completely independent of a priori assumptions, and this factor takes into account how the changing profile shape influences our retrieval.

### 3.4 Space-based constraints on ship emissions

Figure 5c shows a map of OMI tropospheric  $\text{NO}_2$  columns for 2005, gridded on the GEOS-Chem horizontal resolution ( $1/2^\circ \times 2/3^\circ$ ). The conventional approach to constrain the four major ship routes that are visible in the Baltic Sea, North Sea, Bay of Biscay and Mediterranean Sea would be to use the relative difference of simulated and observed columns over these ship routes in combination with the modelled sensitivity  $\beta$ ;

$$E_{\text{top down}} = E_{\text{a priori}} + \left( \frac{N_{\text{OMI}} - N_{\text{GC}}}{N_{\text{GC}}} \right) \cdot \beta \cdot E_{\text{a priori}} \quad (3)$$

In this study we use a first order correction on our  $\text{NO}_x$  emission changes using the dimensionless factor  $\gamma$ , that accounts for an increase in OMI  $\text{NO}_2$  columns when increasing  $\text{NO}_x$  emissions. The new top down  $\text{NO}_x$  emissions inventory we then obtain

19365

## Constraints on ship $\text{NO}_x$ emissions in Europe using GEOS-Chem and OMI

G. C. M. Vinken et al.

Title Page

Abstract

Introduction

Conclusions

References

Tables

Figures

◀

▶

◀

▶

Back

Close

Full Screen / Esc

Printer-friendly Version

Interactive Discussion



by:

$$E_{\text{top down}} = E_{\text{a priori}} + \left( \frac{N_{\text{OMI}} - N_{\text{GC}}}{N_{\text{GC}}} \right) \cdot \beta \cdot E_{\text{a priori}} + \left( \frac{N_{\text{OMI}} - N_{\text{GC}}}{N_{\text{GC}}} \right) \cdot \gamma \cdot \beta \cdot E_{\text{a priori}} \quad (4)$$

For the Baltic Sea, North Sea and Bay of Biscay we provide annual constraints, base on annual averages of filtered days in 2005 and 2006 (see Sect. 2.4 for selection criteria).

For the Mediterranean Sea, more days satisfying our criteria are available, allowing us to provide seasonal constraints for 2005 and 2006.

Using the seasonal and annual averaged tropospheric  $\text{NO}_2$  columns, four along ship track averages were created by averaging the areas in Fig. 5c over the longitude for the Mediterranean Sea and Baltic Sea, and over the latitude for the North Sea and Bay of Biscay (Fig. 7). These averages clearly show enhanced columns relative to the background (of up to  $0.6 \times 10^{15}$  molecules  $\text{cm}^{-2}$ ) over the ship routes. OMI observations indicate that  $\text{NO}_x$  emissions are too low over the Baltic Sea and Bay of Biscay, while emissions are too high over the North Sea and Mediterranean. Furthermore, the cross-section for the Bay of Biscay (Fig. 7, left bottom) shows that emissions in GEOS-Chem are located too far to the east by  $0.5^\circ$  (or  $\sim 50$  km), compared to the OMI observations. These emissions will be relocated in the top down inventory (see next section).

### 3.5 Top down $\text{NO}_x$ ship emissions

We proceed and determine the relative difference of the area under the OMI observed and GEOS-Chem modelled tropospheric  $\text{NO}_2$  cross-sections in Fig. 7. We use this relative difference  $\left( \frac{N_{\text{OMI}} - N_{\text{GC}}}{N_{\text{GC}}} \right)$  to provide constraints following Eq. (4) for the four ship tracks indicated in Fig. 8c. These ship tracks amount to 39% of all ship emissions in the EMEP ship emission inventory for Europe (by mass N). Due to the strong changes in emissions in some ship tracks and strong non-linearities in the  $\text{NO}_x$  chemistry, an additional iteration was needed to match the modelled to simulated columns. This second iteration results in a close match (within 10%) between observed and simulated columns.

## Constraints on ship $\text{NO}_x$ emissions in Europe using GEOS-Chem and OMI

G. C. M. Vinken et al.

Title Page

Abstract

Introduction

Conclusions

References

Tables

Figures

◀

▶

◀

▶

Back

Close

Full Screen / Esc

Printer-friendly Version

Interactive Discussion





**Constraints on ship  
NO<sub>x</sub> emissions in  
Europe using  
GEOS-Chem and OMI**

G. C. M. Vinken et al.

Title Page

Abstract

Introduction

Conclusions

References

Tables

Figures



Back

Close

Full Screen / Esc

Printer-friendly Version

Interactive Discussion

Figure 8 shows the results of our constraints on the ship NO<sub>x</sub> emissions. The OMI top-down total ship NO<sub>x</sub> emissions amount to 0.96 TgN for 2005 (1.0 TgN for 2006), a reduction of 15% (11%) compared to the EMEP inventory. The new inventory (Fig. 8b) is more coherent than the EMEP inventory (Fig. 6d), as sudden stepwise jumps in NO<sub>x</sub> emissions, for instance from the Bay of Biscay to the ship lane west of Portugal, no longer appear in the top-down OMI inventory. Emission totals for the four constrained European seas are given in Table 2, and show that Mediterranean Sea emissions are strongly reduced (to 0.13 TgN) and closely match AMVER-ICOADS emissions (0.12 TgN) for 2005 and 2006. Also the strong emissions in the North Sea are reduced to 0.05 TgN for 2005 (35% lower than EMEP) and are more consistent with emission strengths in the Baltic Sea. Figure 8c shows that the AMVER-ICOADS inventory underestimates emissions in the North Sea and Baltic Sea, and also illustrates that this inventory does not take into account domestic ship traffic in coastal zones. Our top-down emissions are still strong in the English Channel, but our satellite observations do not provide constraints for this area. We note that the TNO-MACC European emission inventory (Denier van der Gon et al., 2011) provides high resolution ship emissions in the North Sea using ship location (Automatic Identification System) data (Jalkanen et al., 2009). OMI top-down emissions for the Baltic Sea and Bay of Biscay are 0.05 TgN for 2005 (131% higher than EMEP) and 0.08 TgN for 2005 (128% higher than EMEP), respectively. The constraints found in this study are also applied to the SO<sub>x</sub> and CO emission inventories, assuming that the scaling in NO<sub>x</sub> emissions is due to increased/decreased activity, and not due to changes in emissions factors.

Using simulations with our new top-down emission inventory, four along ship track averages of observed and simulated NO<sub>2</sub> columns were created (Fig. 9). Compared to Fig. 7, simulated columns now closely match (within 10%) observed columns. Figure 9 also shows the emission strength averaged along the ship tracks. Emissions strengths are similar in the Bay of Biscay and Baltic Sea, but NO<sub>2</sub> column enhancements over ship lanes differ. NO<sub>2</sub> column enhancements are a factor 3–4 lower over the Mediterranean Sea compared to the Baltic Sea and Bay of Biscay, while emissions are only

50 % lower, indicating different photo-chemical regimes (longer NO<sub>2</sub> lifetimes) in different seas in Europe.

### 3.6 Error of the top-down emission inventory

Our approach to derive new top-down ship NO<sub>x</sub> emissions is sensitive to errors in both the satellite observed and simulated NO<sub>2</sub> columns. Important systematic errors in the simulations have been addressed by taking into account the effects of non-linear chemistry in the expanding ship plume, and by changing the location of emissions in the top-down inventory for the Mediterranean Sea and the Bay of Biscay. However, other systematic model errors may still persist, related to errors in the NO<sub>2</sub> chemistry (and hence lifetime), and (vertical) transport (e.g. Lin et al., 2012; Stavrou et al., 2013). Our plume-in-grid method may also introduce errors in our approach, and we cautiously estimate these to be on the order of 15 %. OMI NO<sub>2</sub> observations also have systematic errors, due to errors in the AMFs or stratospheric correction. The error in an OMI observed NO<sub>2</sub> column is estimated to be  $1 \times 10^{15}$  molecules cm<sup>-2</sup> +25 %, and consists of a systematic and random part (Boersma et al., 2011; Irie et al., 2012). We reduce random errors in OMI observations by averaging, but might also introduce an additional error in the background correction of our along ship track averages (Figs. 7 and 9), resulting in an estimate of OMI related errors of 20 %. Assuming the errors in OMI, GEOS-Chem and PARANOX to be largely uncorrelated, and using simple error propagation, we estimate the total systematic component of the errors in our approach to be 29 %. Apart from systematic errors in our model or observations, there are also random errors resulting from our approach. These errors arise from statistical errors in the averaging of the columns and determination of the relative difference between (background corrected) observed and simulated columns. We used the sample standard error to calculate the statistical error in our averages. This error is lowest (30 %) in summer months for the Mediterranean Sea when a large number of observations are available. The statistical error for the North Sea track is largest (70 %), as NO<sub>2</sub> columns



## Constraints on ship NO<sub>x</sub> emissions in Europe using GEOS-Chem and OMI

G. C. M. Vinken et al.

Title Page

Abstract

Introduction

Conclusions

References

Tables

Figures

⏪

⏩

◀

▶

Back

Close

Full Screen / Esc

Printer-friendly Version

Interactive Discussion



satellite observations to changing a priori NO<sub>2</sub> profiles. Although the effect of this sensitivity might be minor for small emission changes, the effect on observed NO<sub>2</sub> columns can be significant for large changes in NO<sub>x</sub> emissions (up to 87 % of GEOS-Chem column change). Our findings stress the need for consistent information in the satellite retrieval and the model, as satellite observations are never fully independent of model information (i.e. vertical NO<sub>2</sub> profiles).

Mediterranean Sea emissions in the top-down inventory (0.13 TgN) closely match the emissions strength of the AMVER-ICOADS inventory (0.12 TgN) for 2005, and emissions in the Bay of Biscay and North Sea appear more coherent with emissions in surrounding seas. Our results indicate that Mediterranean Sea emissions in the EMEP inventory are too high (by 60 %), which could have important consequences for local air quality simulations. Future work could focus on the effect of these reduced and relocated emissions on air quality. For the North Sea, our total top-down emissions amount to 0.05 TgN for 2005 (35 % lower than EMEP). OMI top-down emissions for the Baltic Sea and Bay of Biscay are 0.05 TgN (131 % higher than EMEP) and 0.08 TgN (128 % higher than EMEP) for 2005, respectively. Our top-down emission inventory (0.96 TgN for 2005, 1.0 TgN for 2006) is about 11–15 % lower than the (regional) EMEP ship emission inventory (1.1 TgN), and in closer agreement with the AMVER-ICOADS global emission inventory (0.8 TgN).

Our study provides a framework for future studies to constrain ship NO<sub>x</sub> emissions using satellite NO<sub>2</sub> observations. This may be particularly valuable given the paucity of measurements of ship pollution over open waters, and the upcoming emission control measures. Future work will focus on expanding the analysis to more years, providing an OMI constrained top-down ship NO<sub>x</sub> emissions inventory for use in CTMs. Including observations of additional satellite instruments could also be explored in the future, in order to reduce systematic and random errors in the top-down emissions.

*Acknowledgements.* This research was funded by the Netherlands Organisation for Scientific Research, NWO Vidi grant 864.09.001. We acknowledge the free use of tropospheric NO<sub>2</sub> column data from the OMI from [www.temis.nl](http://www.temis.nl).

## References

- Acarreta, J. R., De Haan, J. F., and Stammes, P.: Cloud pressure retrieval using the  $O_2-O_2$  absorption band at 477 nm, *J. Geophys. Res.-Atmos.*, 109, D05204, doi:10.1029/2003JD003915, 2004. 19360
- 5 Baughcum, S. L., Henderson, S. C., Tritz, T. G., and Pickett, D. C.: Scheduled Civil Aircraft Emission Inventories for 1992: Database Development and Analysis. NASA-CR-4700, National Aeronautics and Space Administration, Langley Research Center, Hampton, VA, USA, 1996. 19357, 19378
- Beirle, S., Platt, U., von Glasow, R., Wenig, M., and Wagner, T.: Estimate of nitrogen oxide emissions from shipping by satellite remote sensing, *Geophys. Res. Lett.*, 31, L18102, doi:10.1029/2004GL020312, 2004. 19354
- 10 Bertram, T. H., Thornton, J. A., Riedel, T. P., Middlebrook, A. M., Bahreini, R., Bates, T. S., Quinn, P. K., and Coffman, D. J.: Direct observations of  $N_2O_5$  reactivity on ambient aerosol particles, *Geophys. Res. Lett.*, 36, L19803, doi:10.1029/2009GL040248, 2009. 19356
- 15 Boersma, K. F., Eskes, H. J., and Brinksma, E. J.: Error analysis for tropospheric  $NO_2$  retrieval from space, *J. Geophys. Res.*, 109, D04311, doi:10.1029/2003JD003962, 2004. 19359, 19361
- Boersma, K. F., Eskes, H. J., Meijer, E. W., and Kelder, H. M.: Estimates of lightning  $NO_x$  production from GOME satellite observations, *Atmos. Chem. Phys.*, 5, 2311–2331, doi:10.5194/acp-5-2311-2005, 2005. 8 19354
- 20 Boersma, K. F., Eskes, H. J., Veefkind, J. P., Brinksma, E. J., van der A, R. J., Sneep, M., van den Oord, G. H. J., Levelt, P. F., Stammes, P., Gleason, J. F., and Bucsela, E. J.: Near-real time retrieval of tropospheric  $NO_2$  from OMI, *Atmos. Chem. Phys.*, 7, 2103–2118, doi:10.5194/acp-7-2103-2007, 2007. 19359
- 25 Boersma, K. F., Eskes, H. J., Dirksen, R. J., van der A, R. J., Veefkind, J. P., Stammes, P., Huijnen, V., Kleipool, Q. L., Sneep, M., Claas, J., Leitão, J., Richter, A., Zhou, Y., and Brunner, D.: An improved tropospheric  $NO_2$  column retrieval algorithm for the Ozone Monitoring Instrument, *Atmos. Meas. Tech.*, 4, 1905–1928, doi:10.5194/amt-4-1905-2011, 2011. 19359, 19368
- 30 Brown, S. S., Dub, W. P., Fuchs, H., Ryerson, T. B., Wollny, A. G., Brock, C. A., Bahreini, R., Middlebrook, A. M., Neuman, J. A., Atlas, E., Roberts, J. M., Osthoff, H. D., Trainer, M., Fehsenfeld, F. C., and Ravishankara, A. R.: Reactive uptake coefficients for  $N_2O_5$  de-

Title Page

Abstract

Introduction

Conclusions

References

Tables

Figures

⏪

⏩

◀

▶

Back

Close

Full Screen / Esc

Printer-friendly Version

Interactive Discussion



**Constraints on ship  
NO<sub>x</sub> emissions in  
Europe using  
GEOS-Chem and OMI**

G. C. M. Vinken et al.

Title Page

Abstract

Introduction

Conclusions

References

Tables

Figures

◀

▶

◀

▶

Back

Close

Full Screen / Esc

Printer-friendly Version

Interactive Discussion

terminated from aircraft measurements during the Second Texas Air Quality Study: comparison to current model parameterizations, *J. Geophys. Res.-Atmos.*, 114, D00F10, doi:10.1029/2008JD011679, 2009. 19356, 19361

5 Butkovskaya, N., Kukui, A., and Le Bras, G.: HNO<sub>3</sub> forming channel of the HO<sub>2</sub> + NO reaction as a function of pressure and temperature in the ranges of 72–600 torr and 223–323 K, *J. Phys. Chem. A*, 111, 9047–9053, doi:10.1021/jp074117m, 2007. 19361

Butkovskaya, N., Rayez, M.-T., Rayez, J.-C., Kukui, A., and Le Bras, G.: Water vapor effect on the HNO<sub>3</sub> yield in the HO<sub>2</sub> + NO reaction: experimental and theoretical evidence, *J. Phys. Chem. A*, 113, 11327–11342, doi:10.1021/jp811428p, 2009. 19361

10 Chen, D., Wang, Y., McElroy, M. B., He, K., Yantosca, R. M., and Le Sager, P.: Regional CO pollution and export in China simulated by the high-resolution nested-grid GEOS-Chem model, *Atmos. Chem. Phys.*, 9, 3825–3839, doi:10.5194/acp-9-3825-2009, 2009. 19356

Corbett, J. J., Winebrake, J. J., Green, E. H., Kasibhatla, P., Eyring, V., and Lauer, A.: Mortality from ship emissions: a global assessment, *Environ. Sci. Technol.*, 41, 8512–8518, 2007. 19354

15 Davis, D. D., Grodzinsky, G., Kasibhatla, P., Crawford, J., Chen, G., Liu, S., Bandy, A., Thornton, D., Guan, H., and Sandholm, S.: Impact of ship emissions on marine boundary layer NO<sub>x</sub> and SO<sub>2</sub> distributions over the Pacific Basin, *Geophys. Res. Lett.*, 28, 235–238, 2001. 19355

20 de Ruyter de Wildt, M., Eskes, H. J., and Boersma, K. F.: The global economic cycle and satellite-derived NO<sub>2</sub> trends over shipping lanes, *Geophys. Res. Lett.*, 39, L01802, doi:10.1029/2011GL049541, 2012. 19354

Denier van der Gon, H., Visschedijk, A., van Gijlswijk, R., and Kuenen, J.: High Resolution European Emission Inventory for the Years 2003–2007, TNO report TNO-060-UT-2011-0058: 49, Utrecht, 2011. 19367

25 Dentener, F., van Weele, M., Krol, M., Houweling, S., and van Velthoven, P.: Trends and inter-annual variability of methane emissions derived from 1979–1993 global CTM simulations, *Atmos. Chem. Phys.*, 3, 73–88, doi:10.5194/acp-3-73-2003, 2003. 19360

Eyring, V., Köhler, H. W., van Aardenne, J., and Lauer, A.: Emissions from international shipping: 1. The last 50 years, *J. Geophys. Res.*, 110, D17305, 2005. 19353

30 Eyring, V., Isaksen, I. S. A., Berntsen, T., Collins, W. J., Corbett, J. J., Endresen, O., Grainger, R. G., Moldanova, J., Schlager, H., and Stevenson, D. S.: Transport impacts on atmosphere and climate: shipping, *Atmos. Environ.*, 44, 4735–4771, 2010. 19353, 19354

**Constraints on ship  
NO<sub>x</sub> emissions in  
Europe using  
GEOS-Chem and OMI**

G. C. M. Vinken et al.

Title Page

Abstract

Introduction

Conclusions

References

Tables

Figures

◀

▶

◀

▶

Back

Close

Full Screen / Esc

Printer-friendly Version

Interactive Discussion

Franke, K., Richter, A., Bovensmann, H., Eyring, V., Jöckel, P., Hoor, P., and Burrows, J. P.: Ship emitted NO<sub>2</sub> in the Indian Ocean: comparison of model results with satellite data, *Atmos. Chem. Phys.*, 9, 7289–7301, doi:10.5194/acp-9-7289-2009, 2009. 19355

5 Hains, J. C., Boersma, K. F., Kroon, M., Dirksen, R. J., Cohen, R. C., Perring, A. E., Bucsela, E., Volten, H., Swart, D. P. J., Richter, A., Wittrock, F., Schoenhardt, A., Wagner, T., Ibrahim, O. W., van Roozendael, M., Pinardi, G., Gleason, J. F., Veefkind, J. P., and Lev-  
elt, P.: Testing and improving OMI DOMINO tropospheric NO<sub>2</sub> using observations from  
the DANDELIONS and INTEX-B validation campaigns, *J. Geophys. Res.*, 115, D05301,  
doi:10.1029/2009JD012399, 2010. 19359

10 Henderson, B. H., Pinder, R. W., Crooks, J., Cohen, R. C., Carlton, A. G., Pye, H. O. T., and  
Vizuete, W.: Combining Bayesian methods and aircraft observations to constrain the HO • +  
NO<sub>2</sub> reaction rate, *Atmos. Chem. Phys.*, 12, 653–667, doi:10.5194/acp-12-653-2012, 2012.  
19361

15 IMO: Revised Marpol Annex VI, Regulation for the prevention of air pollution from ships and  
NO<sub>x</sub> technical code 2008, 2009 Edn., Tech. rep., IMO publishing, London, ISBN 978-92-801-  
4243-3, 2009. 19353

20 IPCC: Climate Change 2007: Impacts, Adaptation and Vulnerability, Contribution of Work-  
ing Group II to the Fourth Assessment Report of the Intergovernmental Panel on Climate  
Change, edited by: Parry, M. L., Canziani, O. F., Palutikof, J. P., van der Linden, P. J., and  
Hanson, C. E., Cambridge University Press, Cambridge, UK, 976 pp., 2007. 19353

Irie, H., Boersma, K. F., Kanaya, Y., Takashima, H., Pan, X., and Wang, Z. F.: Quantitative bias  
estimates for tropospheric NO<sub>2</sub> columns retrieved from SCIAMACHY, OMI, and GOME-2 us-  
ing a common standard for East Asia, *Atmos. Meas. Tech.*, 5, 2403–2411, doi:10.5194/amt-  
5-2403-2012, 2012. 19359, 19368

25 Jaeglé, L., Steinberger, L., Martin, R. V., and Chance, K.: Global partitioning of NO<sub>x</sub> sources  
using satellite observations: relative roles of fossil fuel combustion, biomass burning and soil  
emissions, *Faraday Discuss.*, 130, 407–423, doi:10.1039/b502128f, 2005. 19354

Jalkanen, J.-P., Brink, A., Kalli, J., Pettersson, H., Kukkonen, J., and Stipa, T.: A modelling  
system for the exhaust emissions of marine traffic and its application in the Baltic Sea area,  
*Atmos. Chem. Phys.*, 9, 9209–9223, doi:10.5194/acp-9-9209-2009, 2009. 19367

30 Kasibhatla, P., Levy II, H., Moxim, W. J., Pandis, S. N., Corbett, J. J., Peterson, M. C., Hon-  
rath, R. E., Frost, G. J., Knapp, K., Parrish, D. D., and Ryerson, T. B.: Do emissions from

## Constraints on ship NO<sub>x</sub> emissions in Europe using GEOS-Chem and OMI

G. C. M. Vinken et al.

[Title Page](#)
[Abstract](#)
[Introduction](#)
[Conclusions](#)
[References](#)
[Tables](#)
[Figures](#)




[Back](#)
[Close](#)
[Full Screen / Esc](#)
[Printer-friendly Version](#)
[Interactive Discussion](#)


ships have a significant impact on concentrations of nitrogen oxides in the marine boundary layer?, *Geophys. Res. Lett.*, 27, 2229–2232, 2000. 19355

Kleipool, Q. L., Dobber, M. R., de Haan, J. F., and Levelt, P. F.: Earth surface reflectance climatology from 3 years of OMI data, *J. Geophys. Res.-Atmos.*, 113, D18308, doi:10.1029/2008JD010290, 2008. 19360

Lamsal, L. N., Martin, R. V., Padmanabhan, A., van Donkelaar, A., Zhang, Q., Sioris, C. E., Chance, K., Kurosu, T. P., and Newchurch, M. J.: Application of satellite observations for timely updates to global anthropogenic NO<sub>x</sub> emission inventories, *Geophys. Res. Lett.*, 38, L05810, doi:10.1029/2010GL046476, 2011. 19363, 19364

Lauer, A., Eyring, V., Hendricks, J., Jöckel, P., and Lohmann, U.: Global model simulations of the impact of ocean-going ships on aerosols, clouds, and the radiation budget, *Atmos. Chem. Phys.*, 7, 5061–5079, doi:10.5194/acp-7-5061-2007, 2007. 19353

Lawrence, M. G. and Crutzen, P. J.: Influence of NO<sub>x</sub> emissions from ships on tropospheric photochemistry and climate, *Nature*, 402, 167–170, 1999. 19353

Levelt, P. F., van den Oord en M. R. Dobber, G. H. J., Mälkki, A., Visser, H., de Vries, J., Stammes, P., Lundell, J. O. V., and Saari, H.: The Ozone Monitoring Instrument, *IEEE T. Geosci. Remote*, 44, 1093–1109, doi:10.1109/TGRS.2006.872333, 2006. 19359

Lin, J.-T., Liu, Z., Zhang, Q., Liu, H., Mao, J., and Zhuang, G.: Modeling uncertainties for tropospheric nitrogen dioxide columns affecting satellite-based inverse modeling of nitrogen oxides emissions, *Atmos. Chem. Phys.*, 12, 12255–12275, doi:10.5194/acp-12-12255-2012, 2012. 19356, 19368

Lu, Z. and Streets, D. G.: Increase in NO<sub>x</sub> emissions from indian thermal power plants during 1996–2010: unit-based inventories and multisatellite observations, *Environ. Sci. Technol.*, 46, 7463–7470, doi:10.1021/es300831w, 2012. 19364

Macintyre, H. L. and Evans, M. J.: Sensitivity of a global model to the uptake of N<sub>2</sub>O<sub>5</sub> by tropospheric aerosol, *Atmos. Chem. Phys.*, 10, 7409–7414, doi:10.5194/acp-10-7409-2010, 2010. 19356

Mao, J., Jacob, D. J., Evans, M. J., Olson, J. R., Ren, X., Brune, W. H., Clair, J. M. St., Crouse, J. D., Spencer, K. M., Beaver, M. R., Wennberg, P. O., Cubison, M. J., Jimenez, J. L., Fried, A., Weibring, P., Walega, J. G., Hall, S. R., Weinheimer, A. J., Cohen, R. C., Chen, G., Crawford, J. H., McNaughton, C., Clarke, A. D., Jaeglé, L., Fisher, J. A., Yantosca, R. M., Le Sager, P., and Carouge, C.: Chemistry of hydrogen oxide radicals (HO<sub>x</sub>)



in the Arctic troposphere in spring, *Atmos. Chem. Phys.*, 10, 5823–5838, doi:10.5194/acp-10-5823-2010, 2010. 19356

Marmer, E., Dentener, F., Aardenne, J. v., Cavalli, F., Vignati, E., Velchev, K., Hjorth, J., Boersma, F., Vinken, G., Mihalopoulos, N., and Raes, F.: What can we learn about ship emission inventories from measurements of air pollutants over the Mediterranean Sea?, *Atmos. Chem. Phys.*, 9, 6815–6831, doi:10.5194/acp-9-6815-2009, 2009. 19354, 19363

Martin, R. V., Jacob, D. J., Chance, K., Kurosu, T. P., Palmer, P. I., and Evans, M. J.: Global inventory of nitrogen oxide emissions constrained by space-based observations of NO<sub>2</sub> columns, *J. Geophys. Res.*, 108, 4537, doi:10.1029/2003JD003453, 2003. 19354, 19361

Martin, R. V., Sioris, C. E., Chance, K., Ryerson, T. B., Bertram, T. H., Woolbridge, P. J., Cohen, R. C., Neuman, J. A., Swanson, A., and Flocke, F. M.: Evaluation of space-based constraints on global nitrogen oxide emissions with regional aircraft measurements over and downwind of Eastern North America, *J. Geophys. Res.*, 111, D15308, doi:10.1029/2005JD006680, 2006. 19354

Mollner, A. K., Valluvadasan, S., Feng, L., Sprague, M. K., Okumura, M., Milligan, D. B., Bloss, W. J., Sander, S. P., Martien, P. T., Harley, R. A., McCoy, A. B., and Carter, W. P. L.: Rate of gas phase association of hydroxyl radical and nitrogen dioxide, *Science*, 330, 646–649, doi:10.1126/science.1193030, 2010. 19361

Olivier, J., Peters, J., Granier, C., Pétron, G., Müller, J. F., and Wallens, S.: Present and future surface emissions of atmospheric compounds, POET Report #2, EU project EVK2- 1999-00011, 2003. 19361

Olivier, J. G. J. and Berdowski, J. J. M.: Global emissions sources and sinks, in: *The Climate System*, Lisse, the Netherlands, 33–78 pp., 2001. 19356

Paoli, R., Cariolle, D., and Sausen, R.: Review of effective emissions modeling and computation, *Geosci. Model Dev.*, 4, 643–667, doi:10.5194/gmd-4-643-2011, 2011. 19355

Paxian, A., Eyring, V., Beert, W., Sausen, R., and Wright, C.: Present-day and future global bottom-up ship emissions inventories including polar routes, *Environ. Sci. Technol.*, 44, 1333–1339, 2010. 19354

Richter, A., Eyring, V., Burrows, J. P., Bovensmann, H., Lauer, A., Sierk, B., and Crutzen, P. J.: Satellite measurements of NO<sub>2</sub> from international shipping emissions, *Geophys. Res. Lett.*, 31, L23110, doi:10.1029/2004GL020822, 2004. 19354

**Constraints on ship NO<sub>x</sub> emissions in Europe using GEOS-Chem and OMI**

G. C. M. Vinken et al.

Title Page

Abstract

Introduction

Conclusions

References

Tables

Figures

◀

▶

◀

▶

Back

Close

Full Screen / Esc

Printer-friendly Version

Interactive Discussion

## Constraints on ship NO<sub>x</sub> emissions in Europe using GEOS-Chem and OMI

G. C. M. Vinken et al.

Title Page

Abstract

Introduction

Conclusions

References

Tables

Figures

⏪

⏩

◀

▶

Back

Close

Full Screen / Esc

Printer-friendly Version

Interactive Discussion

- Sauvage, B., Martin, R. V., van Donkelaar, A., and Ziemke, J. R.: Quantification of the factors controlling tropical tropospheric ozone and the South Atlantic maximum, *J. Geophys. Res.*, 112, D11309, doi:10.1029/2006JD008008, 2007. 19357, 19378
- Schreier, M., Mannstein, H., Eyring, V., and Bovensmann, H.: Global ship track distribution and radiative forcing from 1 year of AATSR data, *Geophys. Res. Lett.*, 34, L17814, doi:10.1029/2007GL030664, 2007. 19353
- Sneep, M., de Haan, J. F., Stammes, P., Wang, P., Vanbauce, C., Joiner, J., Vasilkov, A. P., and Levelt, P. F.: Three-way comparison between OMI and PARASOL cloud pressure products, *J. Geophys. Res.-Atmos.*, 113, D15S23, doi:10.1029/2007JD008694, 2008. 19360
- Stavrakou, T., Müller, J.-F., Boersma, K. F., van der A, R. J., Kurokawa, J., Ohara, T., and Zhang, Q.: Key chemical NO<sub>x</sub> sink uncertainties and how they influence top-down emissions of nitrogen oxides, *Atmos. Chem. Phys. Discuss.*, 13, 7871–7929, doi:10.5194/acpd-13-7871-2013, 2013. 19361, 19368
- Valin, L. C., Russell, A. R., Hudman, R. C., and Cohen, R. C.: Effects of model resolution on the interpretation of satellite NO<sub>2</sub> observations, *Atmos. Chem. Phys.*, 11, 11647–11655, doi:10.5194/acp-11-11647-2011, 2011. 19358
- van der Werf, G. R., Randerson, J. T., Giglio, L., Collatz, G. J., Kasibhatla, P. S., and Arellano Jr., A. F.: Interannual variability in global biomass burning emissions from 1997 to 2004, *Atmos. Chem. Phys.*, 6, 3423–3441, doi:10.5194/acp-6-3423-2006, 2006. 19357, 19378
- Vestreng, V.: Review and Revision, Emission data reported to CLRTAP, MSC-W Status Report 2003, Tech. rep., The Norwegian Meteorological Institute, Oslo, Norway, 2003. 19363
- Vestreng, V., Mareckova, K., Kakareka, S., Malchykhina, A., and Kukharchyk, T.: Inventory Review 2007; Emission Data Reported to LRTAP Convention and NEC Directive, MSC-W Technical Report 1/07, Tech. rep., The Norwegian Meteorological Institute, Oslo, Norway, 2007. 19356, 19361, 19362, 19378, 19385
- Vinken, G. C. M., Boersma, K. F., Jacob, D. J., and Meijer, E. W.: Accounting for non-linear chemistry of ship plumes in the GEOS-Chem global chemistry transport model, *Atmos. Chem. Phys.*, 11, 11707–11722, doi:10.5194/acp-11-11707-2011, 2011. 19355, 19357, 19358, 19380, 19381
- Wang, C., Corbett, J. J., and Firestone, J.: Improving spatial representation of global ship emissions inventories, *Environ. Sci. Technol.*, 42, 193–199, 2008. 19356, 19362, 19378, 19385
- Wang, S. W., Zhang, Q., Streets, D. G., He, K. B., Martin, R. V., Lamsal, L. N., Chen, D., Lei, Y., and Lu, Z.: Growth in NO<sub>x</sub> emissions from power plants in China: bottom-up estimates and

satellite observations, *Atmos. Chem. Phys.*, 12, 4429–4447, doi:10.5194/acp-12-4429-2012, 2012. 19354

Wang, X. Y., McElroy, M. B., Jacob, D. J., and Yantosca, R. M.: A nested grid formulation for chemical transport over Asia: applications to CO, *J. Geophys. Res.*, 109, D22307, doi:10.1029/2004JD005237, 2004. 19356

Wang, Y., Jacob, D. J., and Logan, J.: Global simulation of tropospheric O<sub>3</sub>–NO<sub>x</sub>–hydrocarbon chemistry, 1. Model formulation, *J. Geophys. Res.*, 130, 10713–10726, 1998. 19357, 19378

Yevich, R. and Logan, J. A.: An assessment of biofuel use and burning of agricultural waste in the developing world, *Global Biogeochem. Cy.*, 17, 1095, doi:10.1029/2002GB001952, 2003. 19357, 19378

Yienger, J. J., and Levy II, H.: Empirical model of global soil-biogenic NO<sub>x</sub> emissions, *J. Geophys. Res.*, 100, 11447–11464, 1995. 19357

Zhang, L., Jacob, D. J., Knipping, E. M., Kumar, N., Munger, J. W., Carouge, C. C., van Donkelaar, A., Wang, Y. X., and Chen, D.: Nitrogen deposition to the United States: distribution, sources, and processes, *Atmos. Chem. Phys.*, 12, 4539–4554, doi:10.5194/acp-12-4539-2012, 2012. 19356, 19361

## Constraints on ship NO<sub>x</sub> emissions in Europe using GEOS-Chem and OMI

G. C. M. Vinken et al.

Title Page

Abstract

Introduction

Conclusions

References

Tables

Figures

◀

▶

◀

▶

Back

Close

Full Screen / Esc

Printer-friendly Version

Interactive Discussion

## Constraints on ship NO<sub>x</sub> emissions in Europe using GEOS-Chem and OMI

G. C. M. Vinken et al.

Title Page

Abstract

Introduction

Conclusions

References

Tables

Figures

⏪

⏩

◀

▶

Back

Close

Full Screen / Esc

Printer-friendly Version

Interactive Discussion



**Table 1.** Overview of total European 2005–2006 NO<sub>x</sub> emissions used in this study (Tg N yr<sup>-1</sup>)<sup>a</sup>.

Type	Total 2005	Total 2006	Inventory/Source
Anthropogenic	5.4	5.3	EMEP Vestreng et al. (2007)
Aircraft	0.1	0.1	Baughcum et al. (1996)
Biofuel Burning	0.2	0.2	Yevich and Logan (2003)
Fertilizer use	0.3	0.3	Wang et al. (1998)
Ship	1.1	1.2	EMEP & AMVER-ICOADS <sup>b</sup> Vestreng et al. (2007); Wang et al. (2008)
Biomass Burning	0.1	0.1	van der Werf et al. (2006)
Lightning	0.5	0.5	Sauvage et al. (2007)
Soil	0.5	0.5	Wang et al. (1998)
<b>Total</b>	<b>8.3</b>	<b>8.3</b>	

<sup>a</sup> 1 Tg N = 3.29 Tg NO<sub>2</sub>.

<sup>b</sup> Combination of both inventories, see Sect. 3.1 for further details.

**Table 2.** Overview of total ship NO<sub>x</sub> emissions for different seas (ship tracks as defined in Fig. 8b); in the EMEP and AMVER-ICOADS emission inventories, and our OMI top-down inventory for 2005–2006. For the North Sea, Baltic Sea and Bay of Biscay annual constraints are given. More cloud-free observations are available for the Mediterranean Sea and we provide seasonal constraints for this ship track, although winter constraints could not be determined. Beta and gamma values are calculated as indicated in Sect. 3.2. and 3.3.

Area	Season/ Year	Initial relative difference $\frac{N_{\text{OMI}} - N_{\text{GC}}}{N_{\text{GC}}}$	$\beta$ value	$\gamma$ value	EMEP (TgN)	OMI top-down (TgN)	AMVER- ICOADS (TgN)
North Sea	2005	−0.39	0.58	0.59	0.08	0.05	0.23
	2006	−0.32	0.55	0.57	0.08	0.06	0.23
Baltic Sea	2005	1.91	0.25	0.16	0.02	0.05	0.003
	2006	1.99	0.27	0.18	0.02	0.06	0.003
Bay of Biscay	2005	1.01	0.74	0.29	0.04	0.08	0.05
	2006	1.30	0.64	0.26	0.04	0.09	0.05
Mediterranean Sea	Spring 2005	−0.46	0.88	0.64	0.08	0.02	0.03
	Summer 2005	−0.45	0.95	0.84	0.08	0.02	0.03
	Autumn 2005	−0.47	0.81	0.43	0.08	0.03	0.03
	Annual 2005	−0.46	0.88	0.64	0.32	0.10	0.13
	Spring 2006	−0.37	0.85	0.57	0.08	0.03	0.03
	Summer 2006	−0.47	0.8	0.87	0.08	0.02	0.03
	Annual 2006	−0.38	0.79	0.45	0.08	0.04	0.03
	Annual 2006	−0.41	0.81	0.63	0.30	0.13	0.13

[Title Page](#)
[Abstract](#)
[Introduction](#)
[Conclusions](#)
[References](#)
[Tables](#)
[Figures](#)
[⏪](#)
[⏩](#)
[⏴](#)
[⏵](#)
[Back](#)
[Close](#)
[Full Screen / Esc](#)
[Printer-friendly Version](#)
[Interactive Discussion](#)


## Constraints on ship NO<sub>x</sub> emissions in Europe using GEOS-Chem and OMI

G. C. M. Vinken et al.

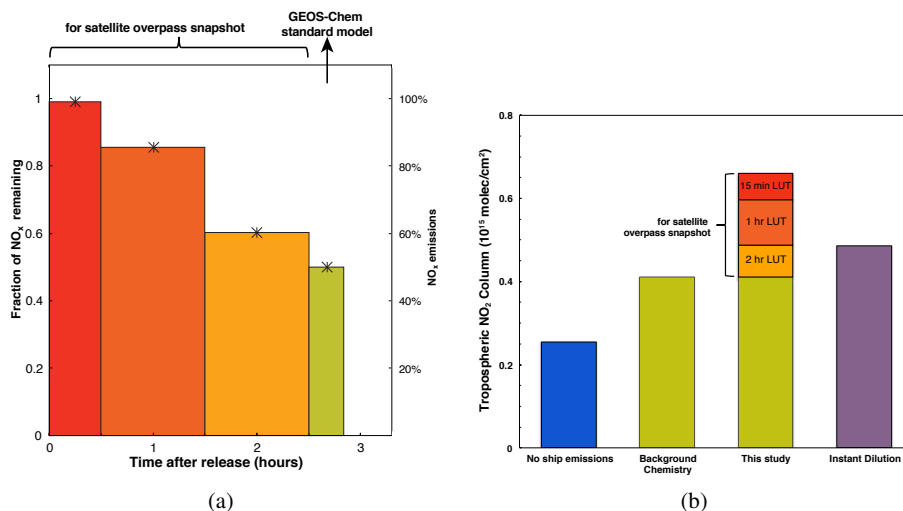


**Fig. 1. (a)** Fraction of NO<sub>x</sub> remaining as a function of time passed since emission. Fractions have been calculated by the PARANOX Gaussian plume model for a grid cell in the Bay of Biscay (averaged between 13:00–15:00) and include the effects of plume expansion and chemistry (Vinken et al., 2011). Resulting emissions used for the model snapshot are the fractions of NO<sub>x</sub> remaining multiplied by the emissions. The green column represents the emissions that are propagated in the regular model chemistry. **(b)** Simulated tropospheric NO<sub>2</sub> columns for a grid cell with ship emissions in the Bay of Biscay at 1 June 2005. Red colours in the third bar represent the contribution to the column from emissions from the last 2.5 h, which are added to the background column to provide model output consistent with a satellite snapshot at 13:30 h. As reference, the tropospheric NO<sub>2</sub> column for this location without ship emissions (blue) and when using instant dilution (purple) are also given.

**Constraints on ship  
NO<sub>x</sub> emissions in  
Europe using  
GEOS-Chem and OMI**

G. C. M. Vinken et al.

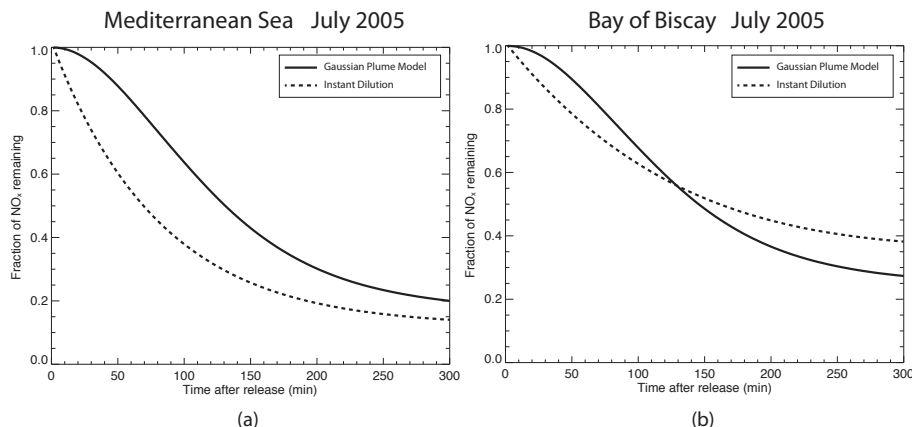


**Fig. 2.** Fraction of NO<sub>x</sub> remaining as function of time calculated by the PARANOX Gaussian plume model (Vinken et al., 2011) for two representative cases in the Mediterranean Sea **(a)** and Bay of Biscay **(b)** for July 2005. The solid line indicates the fraction of NO<sub>x</sub> remaining in an expanding plume with initial size of  $5 \times 5 \text{ m}^2$ , the dashed line represents an initial plume size of  $50 \times 50 \text{ km}^2$  (approximating instant dilution).

[Title Page](#)[Abstract](#)[Introduction](#)[Conclusions](#)[References](#)[Tables](#)[Figures](#)[⏪](#)[⏩](#)[⏴](#)[⏵](#)[Back](#)[Close](#)[Full Screen / Esc](#)[Printer-friendly Version](#)[Interactive Discussion](#)

## Constraints on ship NO<sub>x</sub> emissions in Europe using GEOS-Chem and OMI

G. C. M. Vinken et al.

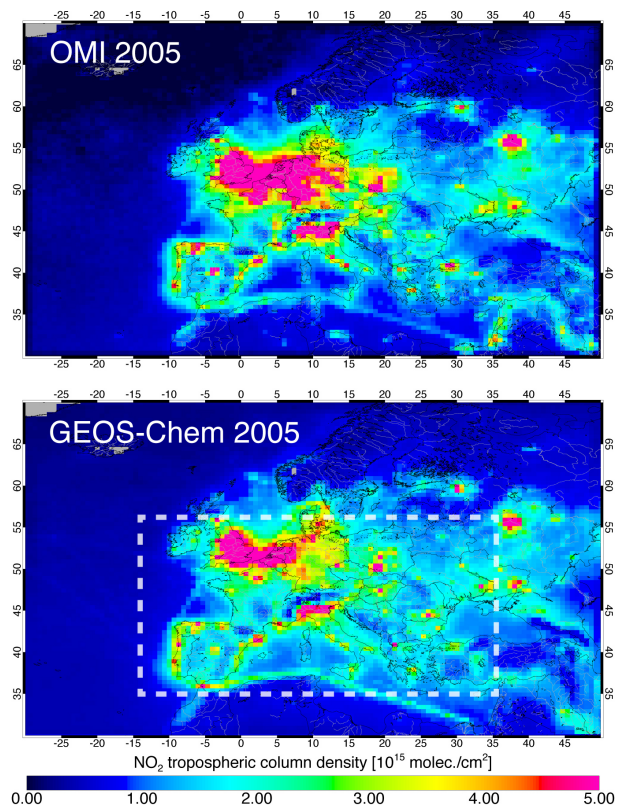


**Fig. 3.** Annual averaged tropospheric NO<sub>2</sub> columns on a  $1/2^\circ \times 2/3^\circ$  resolution for OMI (DOMINO2\_GC, top) and GEOS-Chem (bottom). Pixels with cloud radiance fraction above 0.5, and surface albedo above 0.2 are excluded to reduce retrieval errors. Furthermore the outer 2 pixels on each side of the swath are excluded. OMI pixels are regridded to the GEOS-Chem nested horizontal grid ( $1/2^\circ \times 2/3^\circ$ ), requiring a grid cell coverage of over 75% and more than 3 observations per grid cell. The dashed rectangle indicates the area over which spatial averages of OMI and GEOS-Chem are compared in Sect. 2.3.

[Title Page](#)[Abstract](#)[Introduction](#)[Conclusions](#)[References](#)[Tables](#)[Figures](#)[⏪](#)[⏩](#)[⏴](#)[⏵](#)[Back](#)[Close](#)[Full Screen / Esc](#)[Printer-friendly Version](#)[Interactive Discussion](#)



## Constraints on ship NO<sub>x</sub> emissions in Europe using GEOS-Chem and OMI

G. C. M. Vinken et al.

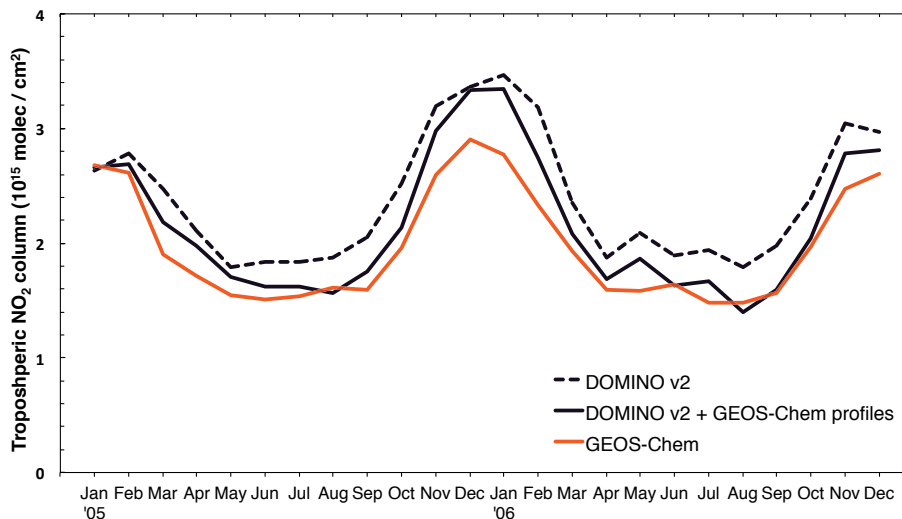


**Fig. 4.** Comparison of monthly averaged OMI and GEOS-Chem tropospheric NO<sub>2</sub> columns for 2005–2006 averaged over (central) Europe defined in Fig. 3. Selection of OMI observations follows the same criteria as Fig. 3.

[Title Page](#)[Abstract](#)[Introduction](#)[Conclusions](#)[References](#)[Tables](#)[Figures](#)[⏪](#)[⏩](#)[⏴](#)[⏵](#)[Back](#)[Close](#)[Full Screen / Esc](#)[Printer-friendly Version](#)[Interactive Discussion](#)

## Constraints on ship NO<sub>x</sub> emissions in Europe using GEOS-Chem and OMI

G. C. M. Vinken et al.

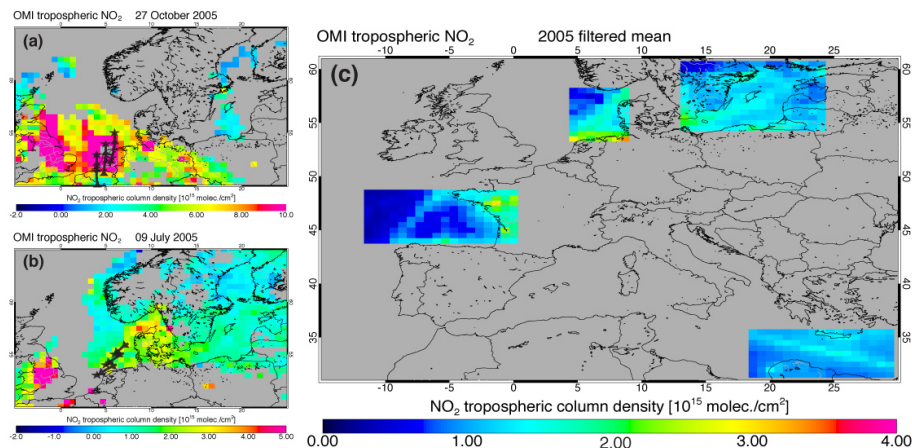


**Fig. 5.** (a) OMI NO<sub>2</sub> observation over the North Sea influenced by outflow from land (note different scale). Back-trajectories with the NOAA-HYSPLIT model show that the North Sea air originated from the Netherlands (black arrows and stars). (b) OMI NO<sub>2</sub> observation with cloud-free observations over the entire North Sea (and Baltic Sea). North Sea air originated from the clean sea for this day (back-trajectories in black arrows and stars). (c) Four ship tracks are visible in the resulting annual average for 2005, after screening out days with strong outflow and partial coverage of the area. The number of days included in this filtered mean is largest for the Mediterranean Sea (about 100), and lower for other seas (North Sea: 20, Baltic Sea: 45, Bay of Biscay: 35).

[Title Page](#)
[Abstract](#)
[Introduction](#)
[Conclusions](#)
[References](#)
[Tables](#)
[Figures](#)
[⏪](#)
[⏩](#)
[⏴](#)
[⏵](#)
[Back](#)
[Close](#)
[Full Screen / Esc](#)
[Printer-friendly Version](#)
[Interactive Discussion](#)

## Constraints on ship NO<sub>x</sub> emissions in Europe using GEOS-Chem and OMI

G. C. M. Vinken et al.

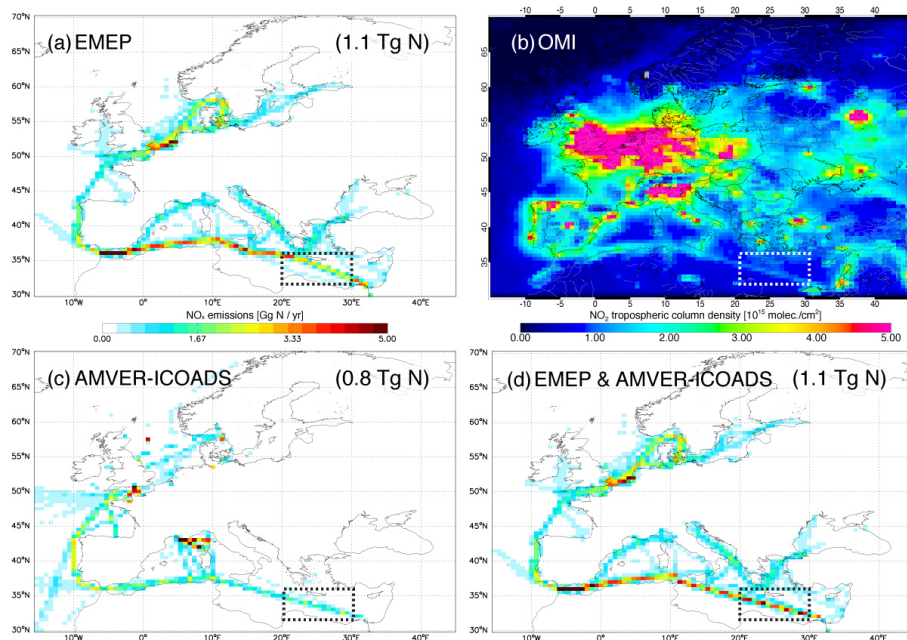


**Fig. 6.** EMEP (Monitoring and Evaluation of the Long-range Transmission of Air Pollutants in Europe) NO<sub>x</sub> ship emission inventory (Vestreng et al., 2007) for 2005, showing emissions in the Mediterranean Sea close to Crete (a, black rectangle). In the AMVER-ICOADS inventory (Wang et al., 2008) for 2001 (c), the location of emissions in the Mediterranean Sea is closer to the ship track location visible in an annual average of OMI tropospheric NO<sub>2</sub> columns for 2005 (b). For this study we created a combination of the EMEP and AMVER-ICOADS inventory, replacing EMEP emissions in the Mediterranean Sea by AMVER-ICOADS emissions, scaled to the EMEP total over this area (d).

[Title Page](#)
[Abstract](#)
[Introduction](#)
[Conclusions](#)
[References](#)
[Tables](#)
[Figures](#)
[◀](#)
[▶](#)
[◀](#)
[▶](#)
[Back](#)
[Close](#)
[Full Screen / Esc](#)
[Printer-friendly Version](#)
[Interactive Discussion](#)

Constraints on ship  
NO<sub>x</sub> emissions in  
Europe using  
GEOS-Chem and OMI

G. C. M. Vinken et al.

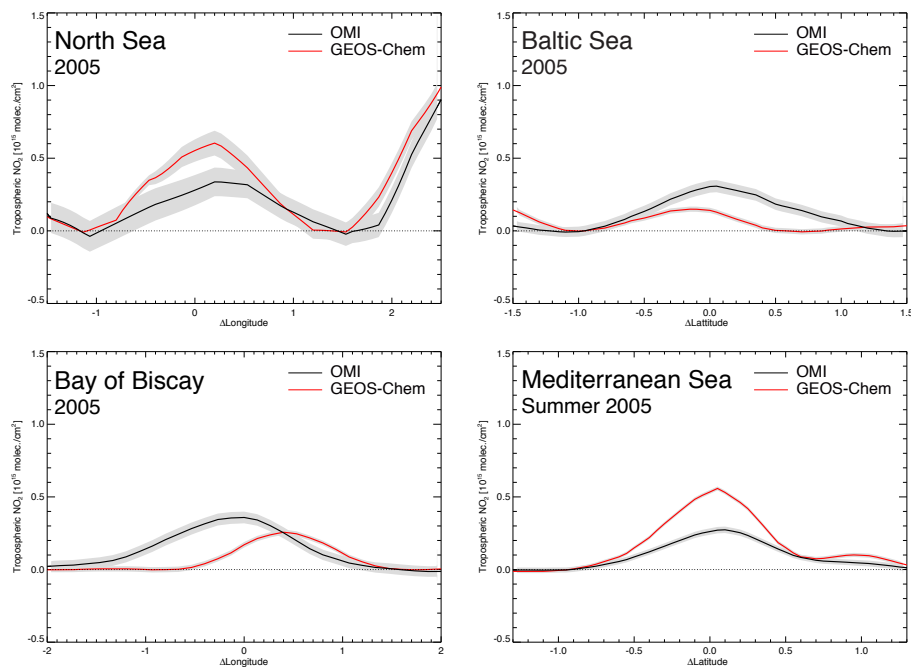


**Fig. 7.** Along ship track averages of tropospheric NO<sub>2</sub> columns over the areas in Fig. 5c for observed columns by OMI (black line), and simulated columns by GEOS-Chem (red line). The area was averaged over the longitude for the Baltic Sea and Mediterranean Sea (upper and bottom right), and over the latitude for the North Sea and Bay of Biscay (upper and lower left). A linear background fit was subtracted from the averages, and grey shadings represent the sample standard error.

[Title Page](#)[Abstract](#)[Introduction](#)[Conclusions](#)[References](#)[Tables](#)[Figures](#)[⏪](#)[⏩](#)[⏴](#)[⏵](#)[Back](#)[Close](#)[Full Screen / Esc](#)[Printer-friendly Version](#)[Interactive Discussion](#)

Constraints on ship  
 $\text{NO}_x$  emissions in  
Europe using  
GEOS-Chem and OMI

G. C. M. Vinken et al.

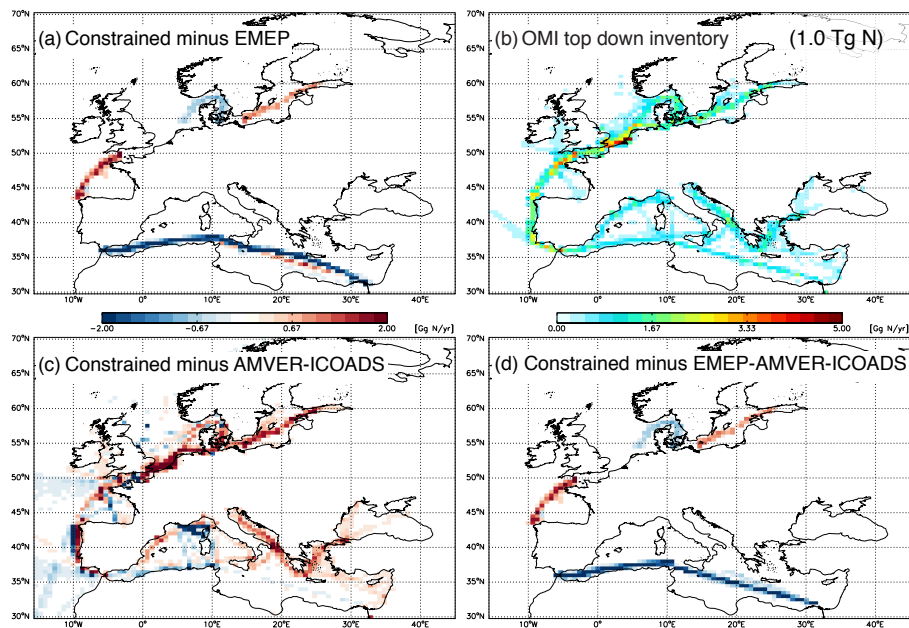


**Fig. 8.** Absolute difference in  $\text{Gg N yr}^{-1}$  between the OMI top-down ship  $\text{NO}_x$  inventory (**b**) and the EMEP-AMVER-ICOADS inventory (**d**), indicating the ship tracks that were constrained in this study. Differences between the new top-down inventory and the (global) AMVER-ICOADS inventory (**c**) show good agreement in the Mediterranean Sea, but also show the lack of domestic ship traffic emissions in coastal waters. Comparison with the original EMEP inventory (**a**) shows the mislocated ship emissions in the Mediterranean Sea, as was discussed in Sect. 3.1.

## Constraints on ship NO<sub>x</sub> emissions in Europe using GEOS-Chem and OMI

G. C. M. Vinken et al.

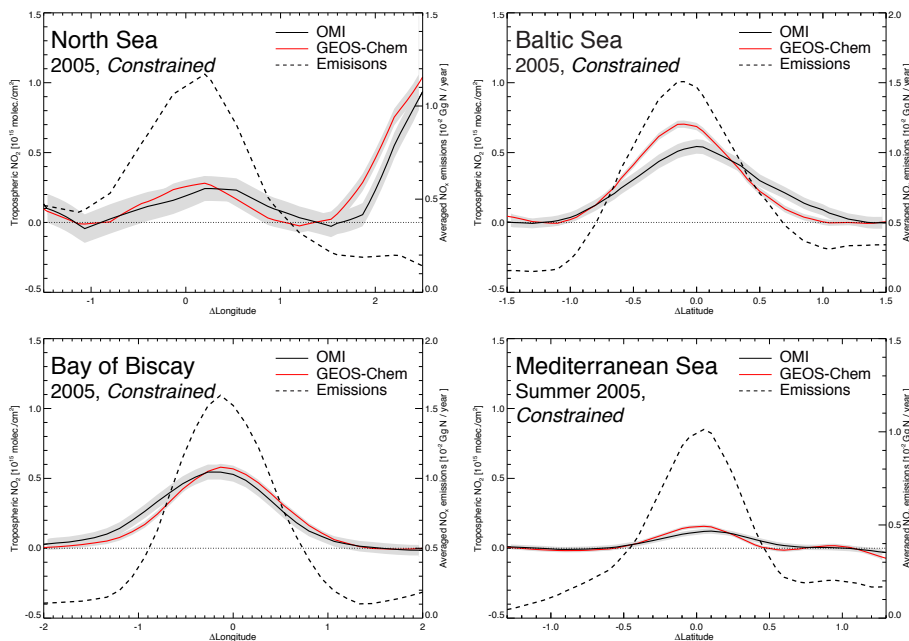


**Fig. 9.** Along ship track averages of the tropospheric NO<sub>2</sub> columns over the areas in Fig. 5c for observed columns by OMI (black line), and simulated columns by GEOS-Chem (red line) using constrained emissions of Fig. 8b. OMI tropospheric NO<sub>2</sub> columns were retrieved using a priori NO<sub>2</sub> profiles simulated with the new top-down emissions. Emissions averaged along the ship track are represented by the dashed line. The area was averaged over the longitude for the Baltic Sea and Mediterranean Sea (upper and bottom right), and over the latitude for the North Sea and Bay of Biscay (upper and lower left). A linear background fit was subtracted from the averages, and grey shadings represent the sample standard error.

Title Page	
Abstract	Introduction
Conclusions	References
Tables	Figures
◀	▶
◀	▶
Back	Close
Full Screen / Esc	
Printer-friendly Version	
Interactive Discussion	